Scripta Materialia, Volume 209, March 2022, Article number 114372
DOI:10.1016/j.scriptamat.2021.114372

Abnormal grain growth in ultrafine grained Ni under high-cycle loading

Alejandro Barrios[a], Yin Zhang[a], Xavier Maeder[b], Gustavo Castelluccio[c]*, Olivier Pierron[a]*, Ting Zhu[a]*

[a] Woodruff School of Mechanical Engineering, Georgia Institute of Technology, Atlanta, GA, 30332, USA

[b] EMPA, Swiss Federal Laboratories for Materials Testing and Research, Laboratory for Mechanics of Materials and Nanostructures, Thun, 3602, Switzerland

[c] School of Aerospace, Transport, and Manufacturing, Cranfield University, Bedfordshire, MK43 0AL, UK

Abstract

Abnormal grain growth can occur in polycrystalline materials with only a fraction of grains growing drastically to consume other grains. Here we report abnormal grain growth in ultrafine grained metal in a rarely explored high-cycle loading regime at ambient temperature. Abnormal grain growth is observed in electroplated Ni microbeams with average initial grain sizes less than 640 nm under a large number of loading cycles (up to 10^9) with low strain amplitudes (< 0.3%). Such abnormal grain growth occurs predominantly in the family of grains whose ⟨100⟩ orientation is along the tensile/compressive loading direction. Micromechanics analysis suggests that the elastic anisotropy of grains dictates the thermodynamic driving force of abnormal grain growth, such that the lowest strain energy density of the ⟨100⟩ oriented grain family dominates grain growth. This work unveils a unique type of abnormal grain growth that may be harnessed to tailor grain microstructures in materials.

Keywords: abnormal grain growth, high-cycle loading, micromechanics, ultrafine grained metal

*Corresponding authors: castellg@cranfield.ac.uk (GC); olivier.pierron@me.gatech.edu (OP); ting.zhu@me.gatech.edu (TZ)

Most technologically important materials are polycrystalline and thus consist of a number of grains separated by grain boundaries (GBs). Grain growth via GB migration is a ubiquitous phenomenon in polycrystalline materials under high thermomechanical loads [1, 2]. If grains grow uniformly over the entire sample, it is called "normal grain growth". On the contrary, when grain growth occurs inhomogeneously, i.e., with only a fraction of grains growing drastically to consume other grains, it is called "abnormal grain growth". Grain sizes and their spatial distribution can strongly influence the physical and chemical properties of materials [3]. Abnormal grain growth can exacerbate degradation and lead to premature failure of materials [4]. Interestingly, abnormal grain growth has been recently harnessed to grow large-area single-crystalline metals that can be further used as substrates to grow large-area single-crystalline two-dimensional materials like graphene for applications in macroelectronics [5]. Hence, understanding grain growth is essential to control grain microstructures for achieving the desired properties of materials.

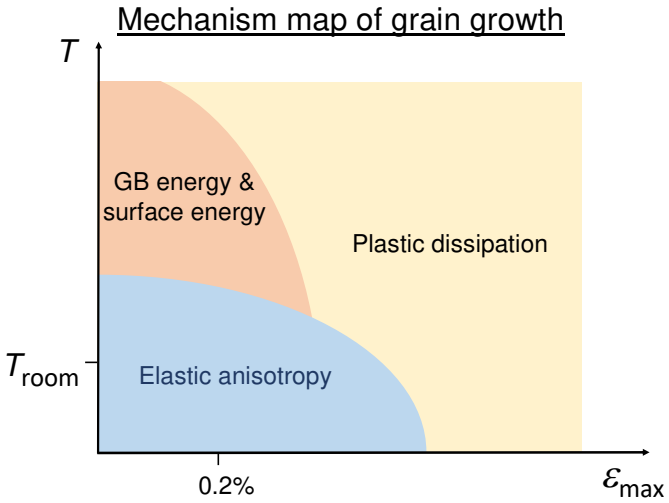

Fig. 1. Schematic mechanism map of grain growth in the space of temperature (T) and maximum strain ($\varepsilon_{\max}$) applied to polycrystalline materials. At relatively low T (around room temperature T_{room}) and $\varepsilon_{\max}$ (around 0.2%) grain growth is driven mainly by a need to release elastic energy and thus dictated by elastic anisotropy of single-crystalline grains. The capillary effects of GB energy and surface energy play an increasing role in driving grain growth with increasing T. In contrast, when $\varepsilon_{\max}$ is large, grain growth is driven mainly by large plastic dissipation.

While both normal and abnormal grain growth have been studied in the past [6-16], here we report the unexpected abnormal grain growth of ultrafine grained (UFG) Ni in a rarely explored high-cycle loading

regime, which involves a large number of cycles (up to 10^9) with low strain amplitudes (< 0.3%), at ambient temperature. We employ a unique MEMS microresonator-based setup to generate high-cycle bending loads on Ni microbeams, such that the largest cyclic tension/compression along the beam's length direction is generated near the beam surface layers where abnormal grain growth is observed. Our micromechanics analysis suggests that the elastic anisotropy of single-crystalline grains in polycrystalline aggregates plays a critical role in the observed abnormal grain growth, albeit with low driving forces of grain growth. The occurrence of such kind of abnormal grain growth is facilitated by the high number of load cycles (up to 10^9) for achieving a pronounced cumulative effect of grain growth. Hence, this unusual grain growth response stands in stark contrast to other previously observed grain growth behaviors under large plastic strains and/or high temperatures [6-16], including those studies under cyclic loading [4, 17-27]. Our results suggest a mechanism map of grain growth as illustrated in Fig. 1, whereby such kind of abnormal grain growth occurs in a special loading regime of temperature T and maximum strain $\varepsilon_{\max}$ applied (highlighted in blue), giving low driving forces of grain growth.

We observed abnormal grain growth in UFG Ni microbeams with a face-centered cubic (fcc) crystal structure under the high-cycle bending load excerted via a MEMS microresonator, at a testing frequency of 8 kHz [28-30]. The microresonator shown in Fig. 2a was fabricated with the MetalMUMPs process from MEMSCAP, which employed a LIGA technique to fabricate an electroplated Ni microbeam of 20 μm thick. Electroplating was performed using a conventional additive-free sulphamate bath at 30 °C, pH = 4, with a direct current (DC) density of 20 mA/cm^2. As a result, a strong [001] fiber texture in the out-of-plane (Z) direction (marked in Fig. 2a) is formed with large columnar grains [31-34]. This is confirmed by the EBSD grain orientation maps in the out-of-plane (Z) and beam's length (X) directions of an untested microbeam, which was obtained from a horizontal cut halfway through the Ni layer thickness (at Z = 10 μm), see Figs. 2b and c. As shown in the ion beam image of the Ni layer sidewall (see Fig. 2a), the bottom 2.5 μm layer has a microstructure of ultrafine equiaxed grains. Fig. 2d and e show the EBSD maps of an untested microbeam from a horizontal cut at Z = 2.5 μm from the bottom of the Ni layer, indicating a [001] fiber

texture in the surface normal direction (also shown with the inverse pole figure (IPF) plots in Fig. 2f). The area-weighted average grain size is less than 640 nm for Z < 2.5 μm, and is ~2 μm in the columnar part of the microbeam (i.e., the top 17.5 μm). Using electrostatic actuation [28, 29], the microbeam can be driven at resonance (~8 kHz), resulting in its cyclic bending deformation. The amplitude of rotation is measured at the beginning of each fatigue test, with a precision of ~ ±1 mrad, and the corresponding strain amplitude at the edges of the microbeam ε_a is determined with a precision of 0.01% [35]. We used these devices over the past decade to investigate the small-scale fatigue behavior of electroplated Ni [35-41]. The fatigue behaviour of these microbeams is mainly dictated by the top 17.5 μm, where the microstructure is columnar. The bottom 2.5 μm layer, with an equiaxed ultrafine grained microstructure, experiences the same loading as the rest of the microbeam. In the following, we show extensive abnormal grain growth occurring *only* in the bottom layer.

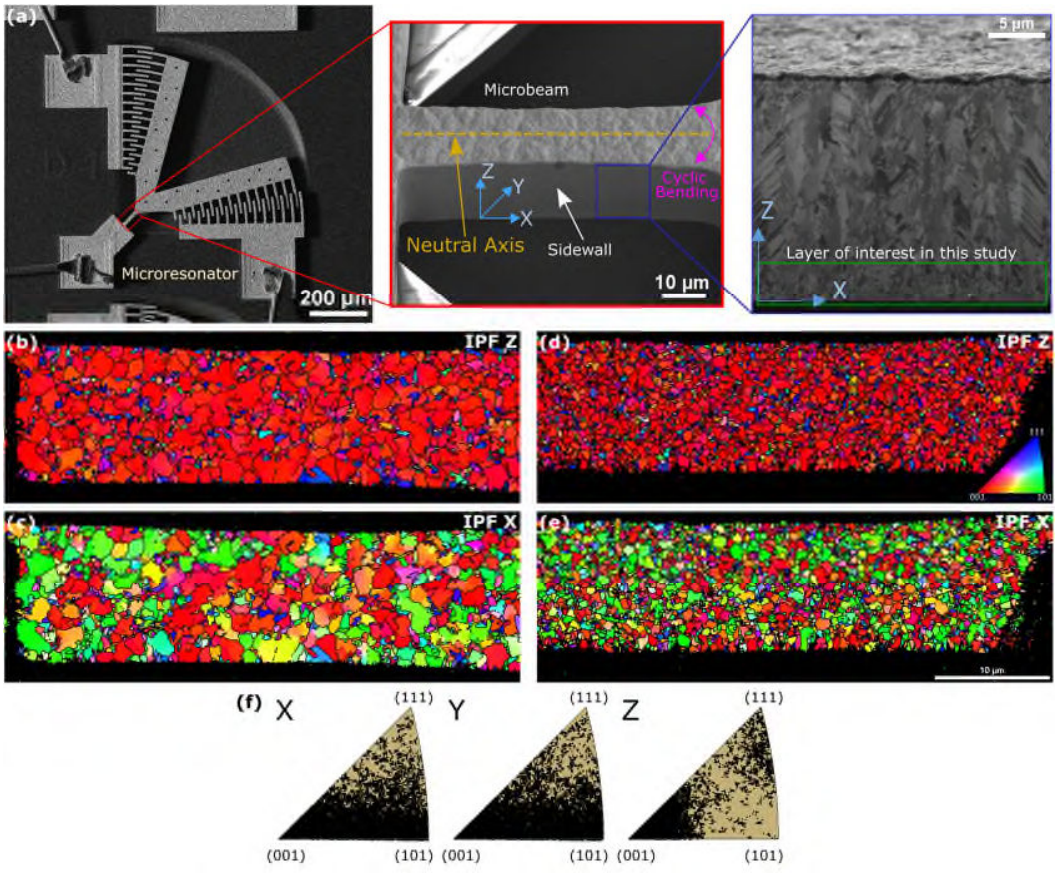

Fig. 2. UFG Ni microbeam under high-cycle loading via a MEMS microresonator. (a) (Left) Ni MEMS microresonator, with (Middle) magnified SEM image of the Ni microbeam, and (Right) ion beam image of the 20-μm-thick Ni layer sidewall showing location of the layer of interest, i.e., within 2.5 μm from the bottom of the microbeam, which contains an equiaxed UFG microstructure. (b) and (c) Grain orientation maps in the out-of-plane (Z) direction and in the beam's length (X) direction, respectively, from an untested microbeam after a horizontal FIB cut halfway through the Ni layer thickness (Z = 10 μm); (d) and (e) Grain orientation maps in the Z and X directions, respectively, from the same untested microbeam after a horizontal FIB cut at ~2.5 μm from the bottom of the Ni layer (Z = 2.5 μm); (f) IPF plots in the X, Y, and Z direction for Ni at ~2.5 μm from the bottom (each black dot represents a pixel from the grain orientation maps).

Abnormal growth of grains preferably along the [100] cyclic tensile/compressive direction (X-axis) is revealed by the band contrast images and the corresponding grain orientation maps in the X direction (IPF-X) for five fatigued specimens (Fig. 3). As noted earlier, these images and maps were taken from horizontal slices at ~1 μm from the bottom of the microbeam. The right column of Fig. 3 lists the number of abnormally large grains (ALG), defined as a size of at least 1 μm, which represents about twice the initial mean grain size (ranging from less than 300 nm at Z = 1 μm to 640 nm at Z = 2.5 μm, due to the gradient in grain size along the Z axis at the bottom of the microbeam; see Fig 2a). Fig. 3a shows a specimen tested at $\varepsilon_a = 0.31\%$ for 1.2×10^7 cycles. Significant abnormal grain growth at such a low ε_a has occurred along the edges of the microbeam, i.e., at the location experiencing the largest amplitude of cyclic tensile/compressive strains in a bent beam. No grain growth occurred within a distance of ~1.5 μm from the neutral axis located at the center of the microbeam (marked by the yellow dashed line in Fig. 3a). Most of the large grains that resulted from deformation-induced grain growth have an elongated shape along the X direction, with a maximum size of ~3 μm in the Y direction. This result indicates that the local strain at a position 3 μm from the edges is not large enough to induce grain growth; the corresponding local strain is estimated approximately as 0.15% for a microbeam width of 12 μm in the Y direction. Some grains become longer than 10 μm in the X direction, suggesting substantial GB migration under the applied cyclic strain. It is important to note that as shown in the grain orientation map in Fig. 3a, most of the large grains have a near [100] orientation in the X direction. This is evidently the result of preferential growth of grains of the [100] orientation by consuming grains of other orientations in the X direction.

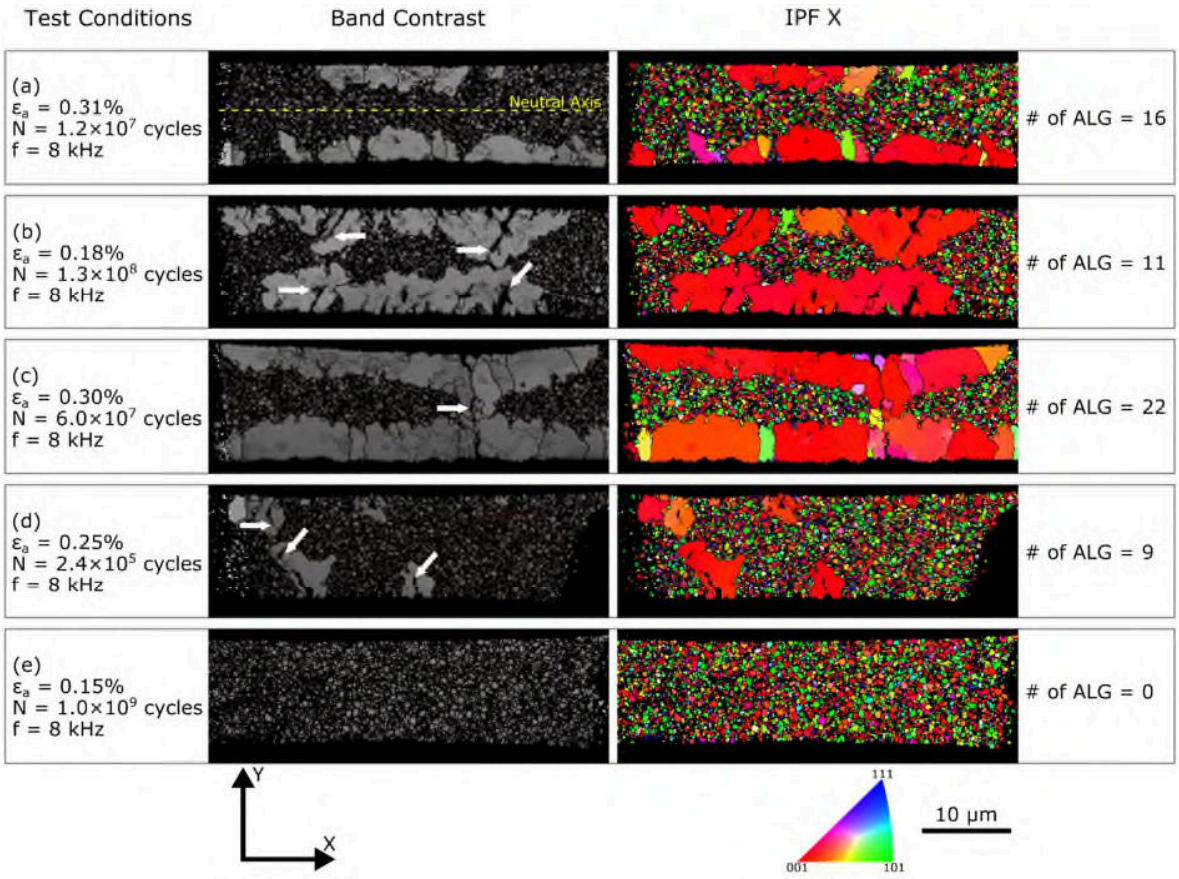

Fig. 3. Abnormal growth of the grains with [100] orientation in the cyclic tensile/compressive loading (X) direction. (a-e) Band contrast images and grain orientation maps in the X direction of horizontal slices obtained at ~1 μm from the bottom of the microbeam for five fatigued specimens. Fatigue-induced cracks are indicated by white arrows.

Fig. 3b presents a specimen tested at $\varepsilon_a = 0.18\%$ for 1.3×10^8 cycles. Similarly, significant abnormal grain growth occurred as well, with elongated shapes along the X direction and a [100] preferential orientation in the X direction. The main difference with Fig. 3a is that the largest grains grew in the Y direction much closer the neutral axis, despite having a lower ε_a (0.18 vs. 0.31%). This is likely the result of fatigue cracks, which accelerate grain growth after a larger number of applied cycles (1.3×10^8 vs. 1.2×10^7) by locally raising the deformation and providing additional driving force, as shown in other studies [42, 43]. Hence, the presence of fatigue cracks can be responsible for the irregular shape of the larger grains

in the Y direction (compared to Fig. 3a). The large grains also exhibit a preferential orientation of [001] in the X direction.

Similar to Fig. 3a, Fig. 3c shows a specimen tested at the same strain level of $\varepsilon_a = 0.3\%$, but for a total number of 6.0×10^7 cycles. This specimen has many large grains with elongated shapes, as long as 10 μm in size in the X direction and 3-4 μm in the Y direction. This specimen has a fatigue crack that initiated from the side of the microbeam. Significant grain coarsening occurred in the fatigue-cracked region, with grains spanning the entire half-width of the microbeam. The large grains also exhibit a preferential orientation of [001] in the X direction.

Fig. 3d presents a specimen tested at $\varepsilon_a = 0.25\%$ for 2.4×10^5 cycles, i.e., at least 50 times less cycling (compared to Figs. 3a-c) for similar ε_a. This sample presents nine ALGs, almost all of which have a [100] preferential orientation in the X direction. However, these ALGs are smaller than those in Fig. 3a-c and none of them have an elongated shape in the X direction. Hence, a significant amount of grain coarsening for the specimens showed in Fig. 3a-c likely occurred between 10^5 and 10^8 cycles, suggesting a continuous growth process for grains with a preferential orientation of [001] in the X direction. The specimen shown in Fig. 3e ($\varepsilon_a = 0.15\%$ for 1.0×10^9 cycles) does not show any grain growth. Hence, there appears to be a threshold of ε_a, between 0.15 and 0.18% (grain growth was observed at 0.18%; see Fig. 3b), below which no grain growth occurs, despite applying up to 10^9 cycles.

Fig. 4 presents in more detail the orientation of ALGs for selected specimens. The left column highlights all the grains with less than 10° misorientation from [001] in the X direction, while the right column only shows the ALGs. Each color in these maps of the right column represents one ALG, and the same color is used in the IPF X plot to show its orientation along the X direction. Comparison of the two maps of the left and right columns from Figs. 4b-e shows that most of the ALGs have a near [001] orientation along X-axis, especially the elongated grains along X-axis. Therefore, these results clearly demonstrate the favorable growth of the [100] grain family along the loading direction. While the bottom portion of the microbeams have a limited number of grains, Fig. 4a shows that there are at least 15-20 grains

along each sidewall (experiencing the largest amplitude of cyclic tensile/compressive strains) along the microbeam length. These 30-40 grains on the two sidewalls are the most likely candidates to become ALGs under cyclic loading, and are sufficient in numbers to provide repeatable results.

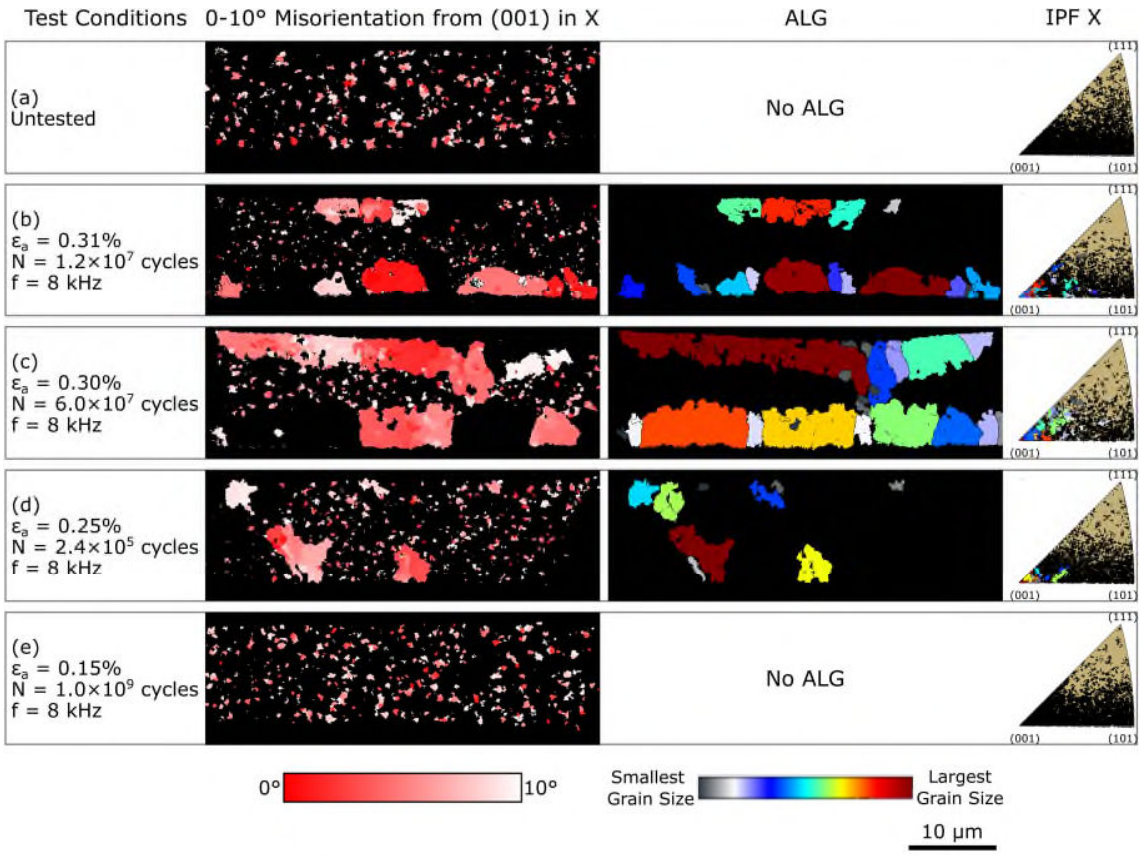

Fig. 4. Grain orientation maps (left column) showing grains whose misorientation from [001] along X is within 10 degree, and grain orientation maps (right column) showing only the ALGs (each orientation represented by a color), along with their location in the IPF X plot, for an untested specimen (a) and four fatigued specimens (b)-(e).

To understand the main finding of abnormal grain growth with a preferential orientation of [001] in the X direction, we developed a micromechanics model to determine the thermodynamic driving force of grain boundary migration as a function of grain orientation. According to Eshelby [44], the thermodynamic driving force of migration of defects and inhomogeneities can be derived using the elastic energy-momentum tensor. For GB migration in a linear elastic material, the thermodynamic driving force per unit

GB area, denoted as F, is given by the jump of $P_{lj}m_l m_j$ normal to the GB plane,

$$F = \Delta\left(P_{lj}m_l m_j\right) = \Delta W - t_i \lambda_i^{\mathrm{T}} \tag{1}$$

where repeated indices imply summation. In Eq. (1), m_i is the unit vector normal to the GB plane; ΔW is the jump of the local elastic strain energy density across the GB; t_i is the continuous traction vector at the GB and given by $\sigma_{ij}m_j$, where σ_{ij} is the stress tensor on one side of the GB; and λ_i^{T} is the transformation strain vector across the GB. We emphasize that ΔW is proportional to the square of stress, while $t_i\lambda_i^{\mathrm{T}}$ is linearly proportional to stress. When *F* is low, the GB velocity is linearly proportional to *F*. As a result, the effect of $t_i\lambda_i^{\mathrm{T}}$ on the average GB velocity becomes zero after a fully reversed load cycle, such that ΔW dictates the average GB velocity and accordingly the direction of GB migration.

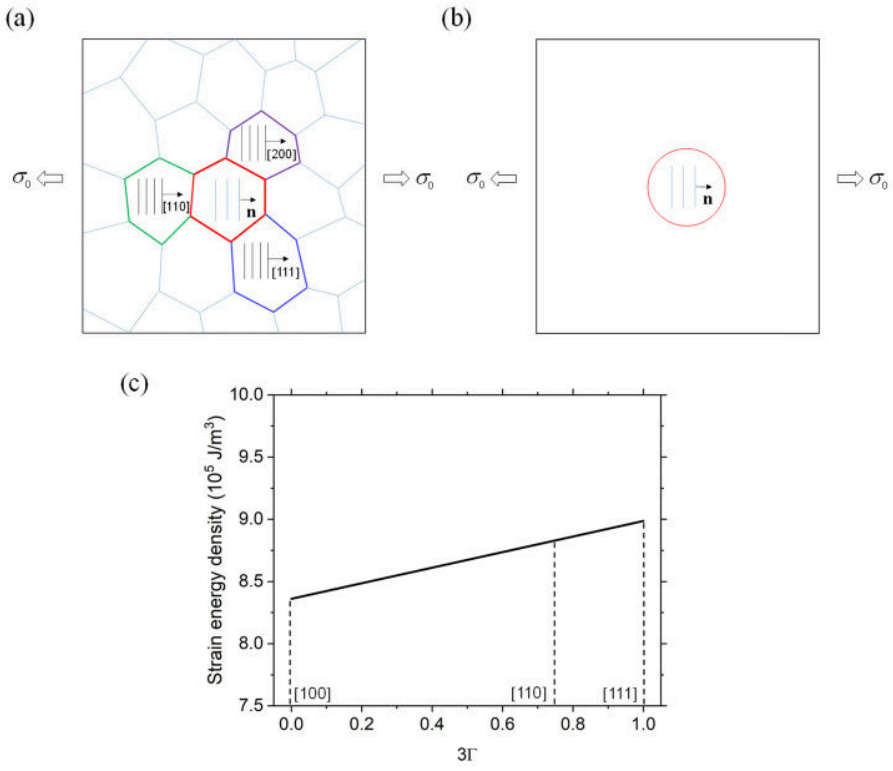

Fig. 5. Micromechanics analysis of the grain orientation effect on strain energy density in polycrystalline Ni under uniaxial tension. (a) Schematic of a polycrystal with random grain orientations. A grain family is

a set of grains with common crystallographic planes (whose unit normal vector is denoted as **n**) along the tensile loading direction. (b) Schematic of the micromechanics model with a representative spherical grain embedded in an effective medium of a polycrystal. (c) Micromechanics results of strain energy density in each grain family as a function of grain orientation index 3Γ under an applied tensile stress of 640 MPa.

We considered a representative spherical grain embedded in a polycrystal (Fig. 5a-b). To determine the stress and strain in this spherical grain, we used a micromechanics model that combines the classical Eshelby inclusion solution [45] and the self-consistent solution of the effective elastic moduli of the polycrystal [46]. While individual grains are elastically anisotropic, the polycrystalline aggregate with a random distribution of grain orientations has the effective isotropic elastic moduli. According to the Eshelby inclusion solution [45], the stress, strain and strain energy density are all uniform in a spherical grain embedded in a homogenized polycrystal. When the polycrystal is subjected to an applied tensile stress σ_0, the uniform strain tensor in this grain is given by

$$\varepsilon_{ij} = U_{ijkl} n_k n_l \sigma_0 \tag{3}$$

where U_{ijkl} is the constrained compliance tensor derived in [46], and n_k denotes the unit vector along the tensile loading direction. Supposing this grain belongs to the [*hkl*] family along the loading direction, we expressed n_k as $(n_1, n_2, n_3) = (h, k, l) / \sqrt{h^2 + k^2 + l^2}$ in the local cubic basis. After algebraic operation of Eq. (3), we derived the uniform strain energy density W in this grain as

$$\begin{aligned} W &= \frac{1}{2} L_{ijkl} \varepsilon_{ij} \varepsilon_{kl} = \frac{\sigma_0^2}{2} L_{ijkl} U_{rsij} n_r n_s U_{pqkl} n_p n_q \\ &= \frac{\sigma_0^2}{2} \left[\frac{3a_{\mathrm{LUU}} + 4b_{\mathrm{LUU}}}{3} - 4\left(b_{\mathrm{LUU}} - c_{\mathrm{LUU}}\right)\Gamma \right] \end{aligned} \tag{4}$$

where $a_{\mathrm{LUU}}, b_{\mathrm{LUU}}$ and c_{LUU} represent the components of the product of $L_{ijkl} U_{rsij} U_{pqkl}$ by using the symbolic tensor notation defined in our previous publication [46]; and Γ is the grain orientation index defined as

$$\Gamma = \frac{h^2k^2 + l^2k^2 + h^2l^2}{\left(h^2 + k^2 + l^2\right)^2} \tag{5}$$

varies between 0 and 1/3 to cover all the grain families with random orientations, and it takes 0, 1/4 and 1/3 for the representative grain families of [100], [110] and [111], respectively. Under an applied stress σ_0 = 640 MPa (corresponding to an applied strain of ~0.31% in our UFG Ni specimens) and with the single-crystal elastic constants of Ni given in [46], Eq. (4) becomes

$$W = \left(8.3607\times10^5 + 1.8768\times10^5 \times \Gamma\right) \text{ J/m}^3 \tag{6}$$

Based on Eq. (6), we plot the linear curve of W versus in Fig. 5c. It is seen that among all the grain orientations along the loading direction, the [100] grain family has the smallest W, while the [111] grain family has the largest W. This grain orientation dependence can be directly correlated to the smallest and largest effective elastic constant of the [100] and [111] grain family along the loading direction, respectively [46]. According to Eq. (1), a GB will migrate favorably from the grain with lower W towards its neighboring grain with higher W, thereby reducing the total elastic strain energy of the polycrystalline aggregate. Hence, the growth of grains in the [100] family is most favorable energetically, which is consistent with the observed abnormal grain growth shown in Figs. 3 and 4. In addition, we have developed a phase-field model that accounts for the strain energy dominated driving force of grain growth and thus produces the direct simulation result of preferential growth of grains in the <100> family, which is consistent with the micromechanics model. This phase-field simulation result will be reported in a follow-up paper.

The above micromechanics analysis is independent of grain size. One effect of having ultrafine grains with high yield strengths is their prevailing high stresses which raise strain energy densities (and accordingly strain energy density differences between neighboring grains) relative to coarse-grained counterparts, thereby increasing the thermodynamic driving force of grain growth to accumulate a sufficient

amount of grain growth observable within a certain load cycles in laboratory experiment. In our theoretical analysis, a grain of certain orientation under consideration is assumed to embed in a homogenized medium of a polycrystalline matrix, and the effective stiffness of this grain is evaluated with respect to the surrounding homogenized matrix. This mean-field analysis can capture the primary effect of elastic anisotropy on the driving force of grain growth. However, direct elastic interactions between neighboring grains are not taken into account in the analysis. As a result, our mean-field solution could not cover cases where neighboring grains have relatively large variations in stiffness, such that their driving forces for grain growth could deviate from the mean-field solution. Nonetheless, our analysis captures the predominant effect of elastic anisotropy on preferential growth of the [100] grain family.

As discussed above, the impact of elastic anisotropy on the abnormal growth of the [100] grain family can be effectively brought out in the high-cycle loading regime at room temperature, as indicated in Fig. 1. If either temperature or maximum applied strain (i.e., low-cycle loading or large monotonic loading) is increased, larger driving forces (due to higher GB energy and mobility, and/or higher plastic dissipation) will instead lead to normal grain growth. Hence, the elastic anisotropy regime illustrated in the mechanism map in Fig. 1 is likely to be confined to low strains and temperatures and therefore low grain growth rates that can only lead to substantial grain growth under large numbers of load cycles. Our MEMS microresonator-based setup facilitates tests in the high-cycle fatigue regime (up to 10^8-10^9 cycles) and thus allows much smaller average grain growth rates, down to 3×10^{-5} nm/cycle, which is likely related to much lower plastic strain amplitudes in the low driving force regime. In this regard, the absence of grain growth at 0.15% can be interpreted as a threshold level in plastic strain amplitude below which GB migration velocity is drastically reduced, despite having a thermodynamic driving force only slightly lower than that at 0.18% (for which grain growth occurred). The kinetics of GB migration under cyclic loading and the underlying mechanisms are still largely unexplored. A modification of the current experimental setup will be pursued to enable *in situ* SEM/EBSD cyclic testing and further investigate the kinetics of grain growth under cyclic loading. We note that similar abnormal grain growth associated with elastic anisotropy was

not observed in recent cycle-induced grain growth studies with different fcc metals, initial grain sizes, and loading conditions [4, 17-27]. Additional studies are therefore required to further understand the low driving force regime of abnormal grain growth illustrated in Fig. 1.

To summarize, this work demonstrates the occurrence of abnormal grain growth under cyclic deformation in the high-cycle fatigue regime. It provides a strong motivation for future investigation of abnormal grain growth behaviors dominated by the effect of elastic anisotropy (as illustrated in Fig. 1) in a variety of material systems by varying composition (e.g., from binary alloys to high-entropy alloys), lattice structure (e.g., from body-centered cubic to complex alloy structures), microstructural geometry (e.g., from bimodal to gradient distributions of grain size), thermomechanical loading (e.g., from liquid nitrogen to high temperatures), among others. Such studies are essential to harnessing this unexpected phenomenon to tailor grain microstructures toward the development of novel high-performance materials.

Acknowledgements

AB, EK, GC, and OP gratefully acknowledge support from NSF through award No CMMI-1562499. Modeling analysis by YZ and TZ was supported by the U.S. Department of Energy, Office of Science, Basic Energy Sciences under Award #DE-SC0018960.

References

[1] M. Hillert, Acta Metallurgica 13 (1965) 227-238.
[2] F.J. Humphreys, M. Hatherly, Recrystallization and Related Annealing Phenomena, Elsevier Science Ltd2002.
[3] Y.M. Wang, M.W. Chen, F.H. Zhou, E. Ma, Nature 419 (2002) 912-915.
[4] Q.S. Pan, J.Z. Long, L.J. Jing, N.R. Tao, L. Lu, Acta Mater. 196 (2020) 252-260.
[5] Q.Q. Ding, Y. Zhang, X. Chen, X.Q. Fu, D.K. Chen, S.J. Chen, L. Gu, F. Wei, H.B. Bei, Y.F. Gao, Nature 574 (2019) 223-227.
[6] C.V. Thompson, R. Carel, J. Mech. Phys. Solids 44 (1996) 657-673.
[7] J. Greiser, P. Mullner, E. Arzt, Acta Mater. 49 (2001) 1041-1050.
[8] D.S. Gianola, S. Van Petegem, M. Legros, S. Brandstetter, H. Van Swygenhoven, K.J. Hemker, Acta Mater. 54 (2006) 2253-2263.
[9] T.J. Rupert, D.S. Gianola, Y. Gan, K.J. Hemker, Science 326 (2009) 1686-1690.
[10] E.A. Holm, S.M. Foiles, Science 328 (2010) 1138-1141.
[11] M. Tonks, P. Millett, W. Cai, D. Wolf, Scr. Mater. 63 (2010) 1049-1052.
[12] M. Tonks, P. Millett, Materials Science and Engineering A 528 (2011) 4086-4091.
[13] P. Sonnweber-Ribic, P.A. Gruber, G. Dehm, H.P. Strunk, E. Arzt, Acta Mater. 60 (2012) 2397-2406.
[14] S.P. Baker, B. Hoffman, L. Timian, A. Silvemail, E.A. Ellis, Acta Mater. 61 (2013) 7121-7132.
[15] E.A. Ellis, M. Chmielus, M.T. Lin, H. Joress, K. Visser, A. Woll, R.P. Vinci, W.L. Brown, S.P. Baker, Acta Mater. 105 (2016) 495-504.
[16] W. Chen, Z.S. You, N.R. Tao, Z.H. Jin, L. Lu, Acta Mater. 125 (2017) 255-264.
[17] H.W. Hoppel, Z.M. Zhou, H. Mughrabi, R.Z. Valiev, Philosophical Magazine a-Physics of Condensed Matter Structure Defects and Mechanical Properties 82 (2002) 1781-1794.
[18] H.W. Hoppel, M. Kautz, C. Xu, A. Murashkin, T.G. Langdon, R.Z. Valiev, H. Mughrabi, Int. J. Fatigue 28 (2006) 1001-1010.
[19] H. Mughrabi, H.W. Hoppel, Int. J. Fatigue 32 (2010) 1413-1427.
[20] O. Glushko, M.J. Cordill, Scr. Mater. 130 (2017) 42-45.
[21] O. Glushko, G. Dehm, Acta Mater. 169 (2019) 99-108.
[22] M.W. Kapp, O. Renk, P. Ghosh, T. Leitner, B. Yang, R. Pippan, Acta Mater. 200 (2020) 136-147.
[23] M.W. Kapp, T. Kremmer, C. Motz, B. Yang, R. Pippan, Acta Mater. 125 (2017) 351-358.
[24] J.Z. Long, Q.S. Pan, N.R. Tao, L. Lu, Scr. Mater. 145 (2018) 99-103.
[25] B.L. Boyce, H.A. Padilla, Metall. Mater. Trans. A-Phys. Metall. Mater. Sci. 42A (2011) 1793-1804.
[26] T.A. Furnish, D.C. Bufford, F. Ren, A. Mehta, K. Hattar, B.L. Boyce, Scr. Mater. 143 (2018) 15-19.
[27] T.A. Furnish, A. Mehta, D. Van Campen, D.C. Bufford, K. Hattar, B.L. Boyce, J. Mater. Sci. 52 (2017) 46-59.
[28] E.K. Baumert, O.N. Pierron, Scr. Mater. 67 (2012) 45-48.
[29] E.K. Baumert, O.N. Pierron, Journal of Microelectromechanical Systems 22 (2013) 16-25.
[30] S. Bhowmick, H. Espinosa, K. Jungjohann, T. Pardoen, O. Pierron, MRS Bulletin 44 (2019) 487-493.
[31] S.W. Banovic, K. Barmak, A.R. Marder, J. Mater. Sci. 33 (1998) 639-645.
[32] A. Godon, J. Creus, X. Feaugas, E. Conforto, L. Pichon, C. Armand, C. Savall, Materials Characterization 62 (2011) 164-173.
[33] S. Pathak, M. Guinard, M.G.C. Vernooij, B. Cousin, Z. Wang, J. Michler, L. Philippe, Surface & Coatings Technology 205 (2011) 3651-3657.
[34] C. Savall, A. Godon, J. Creus, X. Feaugas, Surface & Coatings Technology 206 (2012) 4394-4402.
[35] F. Sadeghi-Tohidi, O.N. Pierron, Acta Mater. 106 (2016) 388-400.
[36] F. Sadeghi-Tohidi, O.N. Pierron, Extreme Mechanics Letters 9 (2016) 97-107.

[37] A. Barrios, S. Gupta, G.M. Castelluccio, O.N. Pierron, Nano Letters 18 (2018) 2595-2602.
[38] E.K. Baumert, F. Sadeghi-Tohidi, E. Hosseinian, O.N. Pierron, Acta Mater. 67 (2014) 156-167.
[39] T. Straub, E.K. Baumert, C. Eberl, O.N. Pierron, Thin Solid Films 526 (2012) 176-182.
[40] E. Kakandar, A. Barrios, J. Michler, X. Maeder, O.N. Pierron, G.M. Castelluccio, Int. J. Fatigue 137 (2020) 105633.
[41] F. Sadeghi-Tohidi, O.N. Pierron, Applied Physics Letters 106 (2015) 201904.
[42] R. Goswami, C.R. Feng, S.B. Qadri, C.S. Pande, Sci Rep 7 (2017) 10179.
[43] R.A. Meirom, D.H. Alsem, A.L. Romasco, T. Clark, R.G. Polcawich, J.S. Pulskamp, M. Dubey, R.O. Ritchie, C.L. Muhlstein, Acta Mater. 59 (2011) 1141-1149.
[44] J.D. Eshelby, J. Elast. 5 (1975) 321-335.
[45] J.D. Eshelby, Proceedings of the Royal Society of London Series A 241 (1957) 376-396.
[46] Y. Zhang, W. Chen, D.L. McDowell, Y.M. Wang, T. Zhu, J. Mech. Phys. Solids 138 (2020) 103899.

Abnormal grain growth in ultrafine grained Ni under high-cycle loading

Barrios, Alejandro

2021-11-02

Barrios A, Zhang Y, Maeder X, et al., (2022) Abnormal grain growth in ultrafine grained Ni under high-cycle loading, Scripta Materialia, Volume 209, March 2022, Article number 114372
https://doi.org/10.1016/j.scriptamat.2021.114372